LANGMUIR

Article

pubs.acs.org/Langmuir

Subnanometric Roughness Affects the Deposition and Mobile Adhesion of *Escherichia coli* on Silanized Glass Surfaces

Sumedha Sharma,[†] Yuly Andrea Jaimes-Lizcano,[†] Ryan B. McLay,[†] Patrick C. Cirino,[†] and Jacinta C. Conrad*[,†,‡]

[†]Department of Chemical and Biomolecular Engineering and [‡]Department of Petroleum Engineering, University of Houston, Houston, Texas 77204-4004, United States

Supporting Information

ABSTRACT: We investigate the deposition and transient adhesion of *Escherichia coli* on alkyl and fluoroalkyl silanized glass surfaces of different carbon chain lengths. The rate at which bacteria deposit onto these surfaces decreases as the shear stress is increased from 3 to 67 mPa, but trends in the deposition rate across all surfaces cannot be predicted from extended DLVO calculations of the interaction potential. As the surface root-mean-square (rms) roughness increases, the deposition rate increases and the percentage of motile tethered cells decreases. Furthermore, on surfaces of root-mean-square roughness of less than 0.2 nm, bacteria exhibit mobile adhesion, for which surface-associated cells linearly translate distances greater than approximately 1.5 times their average body length along the flow direction. *E. coli* bacteria with and without flagella exhibit mobile adhesion, indicating that this behavior is not driven by these appendages. Cells that express fimbriae do not exhibit mobile adhesion. These results suggest that even subnanoscale roughness can influence the deposition and transient adhesion of bacteria and imply that strategies to reduce frictional interactions by making cells or surfaces smoother may help to control the initial fouling of surfaces by *E. coli* bacteria.

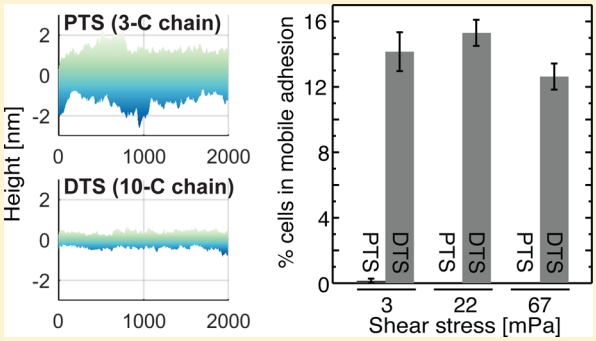

INTRODUCTION

The adhesion of bacteria to a surface represents the first step in the formation of biofilms. These organized and stress-resistant bacterial communities have significant negative impacts in industry, fouling pipelines,[1] ship hulls,[2] and food-processing equipment.[3] Moreover, biofilms foul biomedical devices implanted in the human body,[4] leading to significant costs associated with hospital-acquired infections, and cause or exacerbate diseases in cystic fibrosis[5] and other immunocompromised patients.[6,7] Conversely, biofilm formation aids certain beneficial processes; for example, bacteria can remove harmful contaminants in water purification[8,9] and environmental pollutants in bioremediation.[10,11] For both deleterious and beneficial applications, controlling biofilm formation on surfaces is hence an important goal. Improving the design of materials and strategies toward this goal, in turn, requires understanding the factors that affect the initial attachment of bacteria.

First, bacterial adhesion is mediated by physicochemical interactions, including nonspecific van der Waals, electrostatic, and acid−base interactions between the substrate and bacterium.[12,13] Receptors on the surface of bacteria can specifically interact with particular ligands on the substrate.[14,15] Furthermore, molecules termed adhesins that are present on the cell surface affect bacterial adhesion by complex interaction mechanisms that are yet to be unraveled.[16,17] Thus, the total interaction is influenced by surface properties of bacteria and of substrates. Substrates with amine or aliphatic functional groups typically show higher bacterial deposition than hydroxylic substrates.[18,19] Most bacteria are negatively charged above their isoelectric point,[20] hence bacteria are electrostatically attracted by cationic surfaces[21,22] and repelled by anionic ones.[23] Surface wettability also affects bacterial adhesion. The affinity of bacteria for hydrophobic substrates, for example, is thought to arise from the lower surface energy of bacteria compared to that of the suspending liquid.[24,25] Nonetheless, the role of wettability in cell adhesion is not straightforward: depending on chemistry and cell type, hydrophilic surfaces are reported to exhibit either lower[26−28] or equal[29] numbers of adherent cells compared to hydrophobic surfaces. Finally, superhydrophobic surfaces can have very low bacterial adhesion, as these surfaces exhibit low wettability on short time scales.[30,31]

Second, the roughness of the substrate affects bacterial attachment. On the microscale, increased roughness typically enhances the rate at which bacteria attach and grow.[31,32] This enhancement may arise in part from geometry: bacteria adhering to an irregular substratum may be able to fit into microscale surface features that are comparable to their size,

Received: March 4, 2016
Revised: May 6, 2016
Published: May 9, 2016

DOI: 10.1021/acs.langmuir.6b00883
Langmuir 2016, 32, 5422−5433

thereby protecting themselves from unfavorable environmental factors.[33] On the nanoscale, increased roughness is often correlated with enhanced bacterial attachment for a variety of species, including *Staphyloccocus aureus*,[34,35] *Pseudomonas aeruginosa*,[34,36] and *Escherichia coli*.[35] Other studies, however, report decreasing attachment with nanoscale roughness, for example, for *Pseudoalteromonas issachenkonii* KMM 3549^T.[37] At length scales smaller than 1 nm, very smooth surfaces are thought to inhibit adhesion; few studies address the effect of subnanometric roughness (root-mean-square (rms) roughness of <1 nm) on bacterial attachment. Again, different studies report varying effects of roughness, depending on the chemistry and species—increasing sub-nanometer-scale roughness on polyurethane reduced the attachment of several bacterial species (*Staphylococcus epidermidis*, *E. coli*, and *Proteus mirabilis*)[38] whereas increasing sub-nanometer-scale roughness on titanium did not affect the adhesion of *P. aeruginosa* but reduced the adhesion of *S. aureus*.[39]

Third, hydrodynamic shear forces acting on bacteria under flow conditions affect adhesion. The best-known example of a stress-dependent interaction is the formation of (specific) catch bonds between bacteria type I fimbriae adhesin and surface-attached mannose.[15] The increase in strength of the mannose–fimbriae bond with shear stress led to increased long-duration adhesion. Furthermore, this specific interaction generated the dynamic "stick-and-roll" translational motion of bacteria on mannose- and oligomannose-covered substrates.[15,40,41] Other species also exhibit stress-dependent adhesion, but the mechanisms that mediate these interactions are not known. As one example, shear increased the residence time of *P. aeruginosa* on abiotic surfaces; this interaction did not depend on the substrate and was not mediated by type I pili, type IV pili, flagella, or the extracellular matrix.[42] Even if bacteria do not adhere irreversibly, flow-dependent interactions can give rise to transient or mobile adhesion, which is manifest in *S. epidermidis* bacteria flowing in close proximity to a substrate as surface-associated sliding.[29] This state subsequently transitions over time into immobile adhesion through the development of frictional forces,[43] which are thought to be influenced by local heterogeneities in both substrate and bacterium.[44]

Finally, the interplay between these different factors (surface chemistry, bacterial surface structures, roughness, and flow) can interact to modulate attachment. For example, substratum wettability depends not only on the exposed functional groups but also on the topography.[45] Similarly, the ability of bacteria to attach under flow may be enhanced by roughness-induced frictional interactions that generate effective tangential forces.[43] The flow-driven appearance of transient motility behaviors such as stick-and-roll or mobile adhesion suggests that both surface properties and flow affect the dynamics of attachment; most extant studies, however, quantify attachment only through the cell surface density and not through dynamic measurements of bacteria on surfaces. Hence, there is a need for studies that address the interplay of these competing factors on bacterial attachment and on mobile adhesion.

Here, we show that subnanoscale roughness affects the deposition and transient near-surface motility of *E. coli*. We create model substrates of controlled chemical functionality by assembling layers of organosilanes bearing one of two different terminal functionalities (CH_3– and CF_3–) on glass coverslips and characterize the physicochemical properties of the surfaces. Using confocal imaging and high-throughput tracking algorithms, we quantify the motion of bacteria deposited onto these surfaces from flow. We find that the rate at which bacteria deposit onto a surface generally decreases as the shear stress is increased and cannot be predicted on the basis of extended DLVO calculations. Instead, for a fixed shear stress the deposition rate systematically increases as the surface rms roughness increases, independent of chemical terminal functionality. Similarly, the extent to which surface-tethered cells are able to flip and rotate decreases with rms roughness, consistent with the increased deposition.[19] Finally, we report here the mobile adhesion of *E. coli*, in which cells undergo long linear displacements when located very close to a surface. This behavior occurs in the presence and absence of flagella, suggesting that it is not actively driven. Mobile adhesion depends more strongly on surface roughness than on surface chemistry, appearing on very smooth surfaces of both terminal functionalities, and vanishes when cells express fimbriae. Because mobile adhesion occurs only in the absence of the Velcro-like fimbriae and on very smooth surfaces, we suggest that this behavior occurs only when there is little frictional interaction between the body of a bacterium and the surface. Together, these results suggest that even sub-nanometer-scale roughness affects both transient and irreversible cell adhesion. Hence reducing nanoscale roughness, whether on the cell surface (by inhibiting the expression of fimbriae[46]) or on the substrate, may help to control the initial fouling of surfaces by bacteria.

EXPERIMENTAL SECTION

Bacterial Strains and Plasmids. All strains and plasmids used in the study are summarized in Table 1 and are available upon request. For shear-rate-dependent experiments, we used *Escherichia coli* strain MC1061. To test the effect of bacterial surface structures on deposition, we used *E. coli* strain BW25113 and two isogenic knockout mutants, JW4277 (Δ*fimA*) and JW1908 (Δ*fliC*),[47] that lack the ability to synthesize fimbriae and flagella, respectively. Plasmid pFG10 conferring a constitutive expression of enhanced green fluorescence protein (GFP) and chloramphenicol resistance was introduced into all strains by electroporation. Use of this plasmid allowed cells to be visualized under fluorescence without external labeling. Plasmid pPCC1401 was constructed by cloning the entire *E. coli* MG1655 *fim* operon (genes *fimAICDFGH* were PCR-amplified from genomic DNA) downstream of the *Ptac* promoter (inducible with isopropyl-β-D-1-thiogalactopyranoside (IPTG)) in plasmid pFG1[48] (thus replacing the *araC* gene in pFG1). To test the effect of fimbriae overexpression, strain MG1655Δ*fimA* deficient in fimbriae production (a gift of Prof. Debora Rodrigues, University of Houston) was transformed with plasmid pPCC1401. This transformation resulted in strain MG1655-pPCC1401, which overexpresses fimbriae upon induction with IPTG.

Bacterial Culture. Bacteria were streaked on Luria–Bertani (LB) agar plates (5 g of yeast extract, 5 g of NaCl, 10 g of bactotryptone, and 15 g of agar, all from BD Chemicals) containing an appropriate antibiotic and were incubated overnight at 37 °C (Nuvaire Inc.). Single colonies from the plate were inoculated into sterile LB medium (5 g of yeast extract, 5 g of NaCl, and 10 g of tryptone per 1 L of medium, BD Chemicals) and incubated in an orbital incubator shaker (New Brunswick Scientific) at 200 rpm and 37 °C (for MC1061 and MG1655Δ*fimA*) and 30 °C (for BW25113, JW4277, and JW1908) for approximately 16–17 h. For MC1061, 30 μg/mL chloramphenicol was used in agar plates and cultures. For BW25113, JW4277, and JW1908, 30 μg/mL chloramphenicol and 1 mM IPTG was added to both agar plates and liquid cultures. MG1655Δ*fimA* was grown in LB without any antibiotic. MG1655-pPCC1401 was grown in the presence of apramycin (50 μg/mL) on agar and without shaking in LB for 17 h, followed by induction with 1 mM IPTG for 2 h before harvesting the cells. A dense cell pellet was obtained by centrifuging the cells at 5000*g* in a Sorvall ST 16 centrifuge (Thermo Fisher Scientific). After pelleting, the cells were resuspended in 0.9% NaCl

DOI: 10.1021/acs.langmuir.6b00883
Langmuir 2016, 32, 5422–5433

Table 1. *E. coli* Bacterial Strains Used in This Study

strain (genetic mutation, function)	plasmid	culture protocol	experiments	figures
MC1061	pFG10 (constitutive GFP expression, chloramphenicol resistance)	LB with 30 μg/mL chloramphenicol and 200 rpm shaking at 37 °C for 17 h	flow experiments on all silanized surfaces at three shear stresses (3, 22, and 67 mPa)	3−11, S3
BW25113	pFG10	LB with 30 μg/mL chloramphenicol and 1 mM IPTG, 200 rpm shaking at 30 °C for 17 h	flow experiments on DTS at a single shear stress of 22 mPa	11, S3
JW1908 (Δ*fliC*, deficient in flagella production)	pFG10	LB with 30 μg/mL chloramphenicol and 1 mM IPTG, 200 rpm shaking at 30 °C for 17 h	flow experiments on DTS at a single shear stress of 22 mPa	11, S3
JW4277 (Δ*fimA*, deficient in fimbriae production)	pFG10	LB with 30 μg/mL chloramphenicol and 1 mM IPTG, 200 rpm shaking at 30 °C for 17 h	flow experiments on DTS at a single shear stress of 22 mPa	11, S3
MG1655Δ*fimA* (deficient in fimbriae production)		LB with 200 rpm shaking at 30 °C for 17 h	flow experiments on DTS at a single shear stress of 22 mPa	S3
MG1655-pPCC1401 (MG1655Δ*fimA* transformed with pPCC1401)	pPCC1401 (contains IPTG-inducible fim operon and apramycin resistance)	LB with 50 μg/mL apramycin at 37 °C for 17 h followed by 2 h of incubation with 1 mM IPTG	flow experiments on DTS at a single shear stress of 22 mPa	11, S2, S3

solution (ionic strength 154 mM). Cells were washed two times in NaCl by repeated mixing, centrifuging, and resuspension to remove the growth medium. Pellet washing was limited to one centrifuge cycle for hyperfimbriated MG1655-pPCC1401. Finally, for all imaging experiments, cells were suspended in 154 mM NaCl and diluted to an OD600 of 0.45 measured using a microplate reader (Infinite 200 Pro, Tecan). The harvested cells were in the late stationary stage of growth based on growth curve measurements made for each strain (Figure S1 in Supporting Information).

Microbial Adhesion to Hydrocarbons Test (MATH) and Bacterial Electrophoretic Mobility. The relative hydrophobicity of the cells was measured using the MATH test with *n*-dodecane and hexadecane.[49] All cells were hydrophilic and minimally adhered to hydrocarbons, as shown in Table 2. Zeta potentials for the *E. coli* strains in 154 mM NaCl were measured using a NanoBrook ZetaPALs (Brookhaven Instruments) ζ-potential analyzer. All cells were negatively charged under the experimental conditions used in flow studies.

Table 2. Relative Hydrophobicity and Zeta Potentials for the Bacterial Strains Used in This Study[a]

strain	% hydrophobicity (std deviation) *n*-dodecane	% hydrophobicity (std deviation) hexadecane	zeta potential (mV) (std deviation)
MC1061	9 (1)	7 (4)	−23 (2)
BW25113 (wild type)	3 (1)	3 (1)	−20 (4)
JW4277 (Δ*fimA*)	4 (2)	5 (2)	−19 (4)
JW1908 (Δ*fliC*)	7 (3)	3 (3)	−17 (3)

[a]Numbers in parentheses correspond to the standard deviation over at least three replicate measurements.

Flagellar Expression. The expression of flagella for MC1061, BW25113, and JW4277 strains (or the absence of flagella in JW1908) was confirmed by a bacteria motility assay[50] (on a 0.3% agar plate) and by microscopic observation of swimming motility (or lack of swimming motility).

Fimbrial Expression. All strains were tested for the expression of type 1 fimbriae by confocal microscopy and fluorescence conjugated antibody binding using PAb49 (courtesy of Prof. Evgeni Sokurenko and Prof. Wendy Thomas, University of Washington) and Alexa Fluor 568 conjugated secondary antibody (Thermo Fisher Scientific) (Section S1 and Figure S2 in Supporting Information). First, PAb49 (the anti-*fimA* antibody derived from rabbit serum) was allowed to bind to the fimA protein on fimbriae. Next, the goat-derived antirabbit IgG secondary antibody−Alexa Fluor 568 conjugate was allowed to bind to PAb49 so that the fluorescently labeled fimbriae could be visualized using fluorescence confocal microscopy. All strains were also tested for the expression of fimbriae using transmission electron microscopy (JEOL 1200 EX) (Figure S3 in Supporting Information).

Substrate Preparation. To prepare the test substrates for flow experiments, we used silanes bearing one of two different terminal surface chemistries, CH_3− or CF_3−, and varied the C-chain length from 3 to 18 or from 3 to 10, respectively (Figure 1). All organosilanes were purchased from Gelest and were deposited from solution onto glass coverslips. Prior to deposition, coverslips of dimensions 48 × 65 mm^2 (thickness 0.13−0.17, Gold Seal) were cleaned by sonication in acetone (Macron, AR grade) followed by deionized (DI) water (resistivity 18.2 MΩ·cm, Millipore water purification system), dried under nitrogen, and then exposed to air plasma (Harrick Plasma) for 2 min. To deposit 1*H*,1*H*,2*H*,2*H*-perfluorodecyltrichlorosilane (FDTS) and 3,3,3-trifluoropropyltrichlorosilane (FPTS), plasma-treated glass slides were immersed in isooctane (Sigma-Aldrich) for 10 min and then transferred to a 1 mM solution of either FDTS or FPTS in isooctane that had been mixed by sonication for 5 min. After allowing deposition to proceed for 10 min, the slides were successively rinsed with isooctane, isopropanol, and DI water. To deposit octadecyltri-

DOI: 10.1021/acs.langmuir.6b00883
Langmuir 2016, 32, 5422−5433

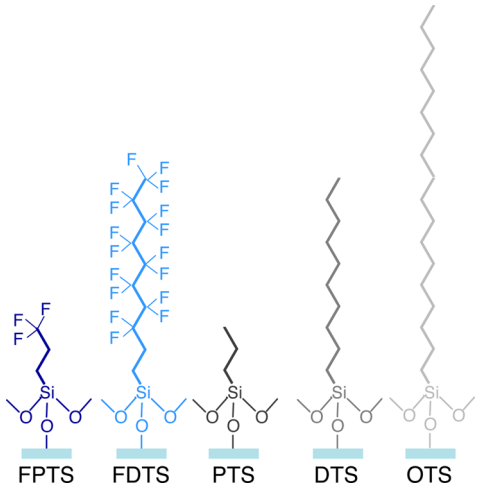

Figure 1. Chemical structures of the organosilanes used to create glass surfaces of controlled chemistry used in this study.[52]

chlorosilane (OTS), *n*-decyltrichlorosilane (DTS), and propyltrichlorosilane (PTS), slides were immersed in a 1 mM solution of OTS, DTS, or PTS in hexane (Sigma-Aldrich) for 2 h. Slides were then sonicated successively in chloroform (Sigma-Aldrich), acetone (Macron), and DI water for 2 min each. After deposition and rinsing, all surfaces were dried under nitrogen and then baked at 110 °C. Silanized substrates were placed in Petri dishes, sealed with Parafilm, and stored in a desiccator for no more than 1 day before use in flow experiments.

Surface Characterization. Water contact angles for each silanized surface were measured using a Dataphysics OCA 15EC goniometer. Contact angles for two other test liquids, ethylene glycol (99%, Alfa Aesar) and diiodomethane (99%, Alfa Aesar), were measured for each surface, and the surface energy was calculated using the method of van Oss.[51] The thickness of the silane layers was estimated by measuring the thickness for equivalent silane depositions made on a Si wafer using spectroscopic ellipsometry (M-2000, J.A. Woolam). All measurements were performed at an angle of 70°. The reported data correspond to at least five spot measurements made on three samples.

The presence of chemical groups attached to the surfaces was confirmed using X-ray photoelectron spectroscopy (S3) (Physical Electronics model 5700) using an Al Kα X-ray source (1486.6 eV) under ultrahigh vacuum. The takeoff angle was 45°, and the analyzer spot diameter was 800 μm. Survey and high-resolution spectra were recorded at pass energies of 187.85 and 23.5 eV, respectively. The binding-energy scales were referenced to 284.6 eV, corresponding to the maximum intensity for a C 1s spectrum. Spectral analysis and peak fitting were performed using the Multipak software package (Multipak V5.0A, Physical Electronics, Inc.). Atomic compositions were estimated from the high-resolution scans.

Atomic force microscopy (AFM; Nanoscope IV, Digital instruments) was used to measure the surface roughness of silanized glass surfaces. In a typical experiment, a 4 μm^2 area was scanned at 2 Hz in tapping mode in air using an n-type silicon cantilever (μMasch, resonance frequency = 320 kHz, force constant = 40 N/m). AFM images were analyzed using NanoScope 6.13R1 software to calculate roughness parameters. Error bars correspond to standard deviations from at least five spot measurements made on at least two surfaces.

To characterize the zeta potentials of silanized surfaces, silanes were deposited on silica nanoparticles (diameter of 170 nm) following the protocols given earlier for surfaces. The zeta potentials of the silanized nanoparticles suspended in 154 mM NaCl were measured using a NanoBrook ZetaPALs (Brookhaven Instruments) ζ-potential analyzer.

Flow Experiments and Image Analysis. Suspensions of cells were allowed to flow through a linear channel using a syringe pump (model 11, Harvard Apparatus) at applied flow rates of Q = 7.5, 60, and 180 mL/h. The shear stress at the wall was $\sigma = 3Q\mu/2Wb^2$, where μ is the viscosity of water (0.89 mPa·s) and W = 4 mm and $2b$ = 1 mm are the width and height, respectively, of the flow channel; in these experiments, σ varied from 3 to 67 mPa (1 mPa = 1 pN/μm^2). Cells containing the fluorescent plasmid (pFG10) that were deposited on the surfaces during flow were imaged using a confocal fluorescence scanner (VT Infinity, Visitech) attached to a Leica DM4000 inverted microscope that was equipped with a 100× oil immersion lens (HCX PL APO of numerical aperture 1.4). A laser excitation source with an excitation wavelength of λ = 488 nm was used to excite the constitutively expressed GFP in the cells. One image with an exposure time of 0.3 s and a pixel size of 0.125 ± 0.0006 μm was acquired every 3 s using an ORCA 200 camera (Hamamatsu) that was controlled by Voxcell Scan software (Visitech). In a typical flow experiment, 300 images with an area of 84 × 64 μm^2 (corresponding to 672 pixels × 512 pixels) were acquired over a total time of 15 min. Experiments on each silanized surface were performed in triplicate on at least two different surfaces with at least two different bacterial cultures. For experiments involving MG1655Δ*fimA*, which did not contain the fluorescent plasmid, bacteria were imaged using brightfield microscopy and an Olympus DP21 camera. For experiments involving hyperfimbriated strain MG1655-pPCC1401, cells were imaged with brightfield microscopy (using nonlabeled cells) and with confocal fluorescence scanning (using cells labeled with 300 nM Syto 9 nucleic acid stain (ThermoFisher)).

Algorithms written in IDL (Exelis VIS)[53] were used to locate and track single cells in a time series of microscopy images. Additional analyses of cell attachment and detachment rates, speed, and residence time of cells in mobile adhesion were performed using routines written in Matlab (MathWorks) and in IDL.

RESULTS AND DISCUSSION

Surface Characterization. To generate well-characterized surfaces for bacterial adhesion experiments, we deposit silanes of two different terminal functionalities (CH_3– and CF_3–) and lengths of the carbon (C) chain (3, 10, and 18). We measure the water contact angle (WCA), surface energy, thickness, and zeta potential of the different surfaces, as summarized in Table 3. All surfaces except FPTS are hydrophobic, as assessed from the water contact angle, and exhibit thicknesses that are consistent with multilayer formation. To characterize the surface roughness, we obtain AFM images for each sample. The roughness of the different surfaces varies with silane

Table 3. Water Contact Angle, Surface Energy, Thickness, Zeta Potential, and Roughness of Silanized Glass Surfaces[a]

substrate	WCA (deg)	surface energy (mJ/m^2)	thickness (nm)	ζ potential (mV)	rms roughness (nm)
FPTS	78 (3)	30 (1)	1.99 (0.04)	−29 (2)	0.73 (0.1)
FDTS	110 (1)	12 (1)	1.63 (0.02)	−31 (2)	0.16 (0.02)
PTS	92 (2)	29 (1)	1.67 (0.08)	−17 (2)	0.68 (0.08)
DTS	106 (3)	23 (1)	1.67 (0.03)	−26 (2)	0.17 (0.03)
OTS	112 (2)	20 (2)	3.10 (0.2)	−16 (1)	0.51 (0.2)

[a]Numbers in parentheses correspond to standard deviations over five spot measurements made on at least three surfaces for WCA, surface energy, and thickness; five aliquots per sample for zeta potential; and five spot scans on two surfaces for roughness.

DOI: 10.1021/acs.langmuir.6b00883
Langmuir 2016, 32, 5422−5433

chemistry, as shown in representative images in Figure 2, but is reproducible between different preparations. From the AFM

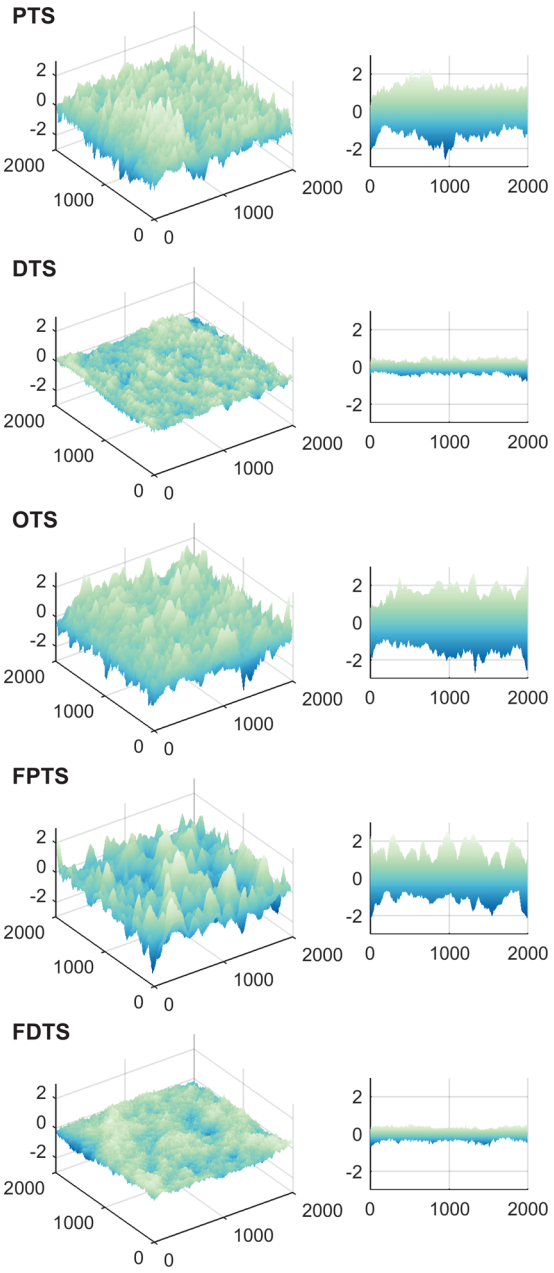

Figure 2. AFM images (left) and height maps (right) for the five silanized surfaces bearing either a $-CH_3$ or $-CF_3$ terminal group and a C-chain length of 3, 10, or 18. Lengths (on the x and y axes) and heights (on the z axis) are given in nanometers. The FDTS ($-CF_3$, C-10) and DTS ($-CH_3$, C-10) surfaces exhibit lower AFM rms roughnesses than do FPTS (C-3), PTS (C-3), and OTS (C-18) surfaces of similar terminal functionality.

images, we calculate the root-mean-square (rms) roughness reported in Table 3 as well as the average (R_a), 10-point average (R_z), and maximum peak-to-valley (R_{max}) roughnesses (Table S6 in Supporting Information). The DTS and FDTS (C-10) surfaces exhibit an rms roughness of less than 0.2 nm, more than a factor of 2 lower than for all other surfaces of similar chemistry and hydrophobicity. These roughnesses are consistent with those obtained in earlier AFM measurements[54] and molecular simulations[55] for these silanes. Finally, we characterize the surface elemental composition using X-ray photoelectron spectroscopy (XPS) (Section S3 in the Supporting Information). The chemical groups expected from each silane structure are observed in the XPS spectra (Figures S4 and S5), confirming that in each case we successfully form silane layers on the glass coverslips. Furthermore, no surface contaminants are identified in the XPS analysis. We therefore conclude that our deposition protocols produce reproducible and (to the best of our ability to determine) contaminant-free multilayers.

Bacterial Deposition. Subsequently, we allowed bacteria to flow through linear microchannels and deposit on the silanized surfaces. For all surfaces, the deposition rate generally decreases with shear stress across the range of shear stresses investigated, as shown in Figure 3. The alkyl- and fluoroalkyl-silane surfaces

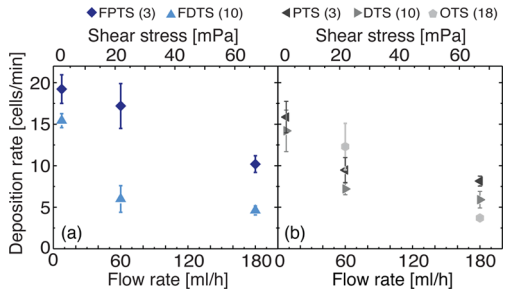

Figure 3. Deposition rate (cells/min) as a function of flow rate (bottom x axis) or shear stress (top x axis) for long-chain (C-18 and C-10) and short-chain (C-3) (a) fluoroalkylsilanes and (b) alkylsilanes on glass. Error bars indicate the standard deviation over three replicates. Strain: MC1061.

exhibit slightly different dependences of deposition rate on chain length: the deposition rate on fluoroalkyl surfaces varies with C-chain length (Figure 3a), whereas the deposition rate does not depend on the C-chain length for the alkyl surfaces (Figure 3b).

To understand the variation of the deposition rate on the different surfaces, we first estimate the interaction potential between *E. coli* MC1061 bacteria and each silanized substrate using the extended-Derjaguin–Landau–Verwey–Overbeek (xDLVO) theory. The xDLVO potential models the van der Waals, electrostatic, and acid–base interactions between the surface and a rigid spherical bacterium. (A full description of the xDLVO calculations is given in the Supporting Information in Section S4.) The xDLVO calculations predict that *E. coli* MC1061 bacteria experience a strong repulsive interaction upon contacting the long-chain (C-10 or C-18) FDTS, DTS, and OTS surfaces but an attractive interaction upon contacting the short-chain (C-3) FPTS or PTS surfaces (Figure 4). Our experimental results show that bacteria deposit less on FDTS, DTS, and OTS surfaces than on FPTS surfaces, but the experimentally observed deposition on PTS is less than expected on the basis of the energy calculations. The discrepancies between the energy calculations and the observed deposition patterns suggest that other features on the bacterial surface or silanized substrate affect adhesion. We therefore look for other surface properties that better correlate with observed adhesion.

The AFM images in Figure 2 reveal significant variations in roughness of the different surfaces. The DTS and FDTS surfaces, in particular, exhibit rms roughnesses of less than 0.2 nm, more than a factor of 2 lower than for all other surfaces of similar chemistry and hydrophobicity (Table 3). We therefore

DOI: 10.1021/acs.langmuir.6b00883
Langmuir 2016, 32, 5422–5433

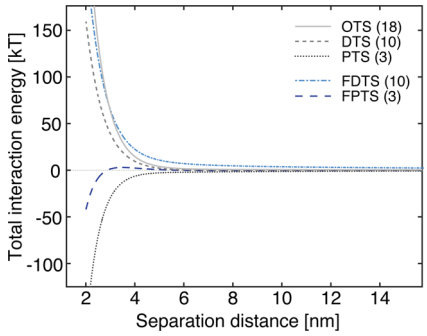

Figure 4. Estimated total interaction potential as a function of the separation distance of bacteria from the surface, calculated from xDLVO theory for a sphere−plate interaction for *E. coli* MC1061 and five silanized glass surfaces in suspensions of 154 mM ionic strength. Colors for each surface correspond to those used in Figure 1.

surmise that this sub-nanometer-scale roughness, in addition to shear stress and interaction energy, affects bacterial deposition. To test this idea, we examine the dependence of the deposition rate on the rms roughness. For a given shear stress, the deposition rate generally increases with the rms roughness, as shown in Figure 5, with a dependence that is less pronounced than that of shear.

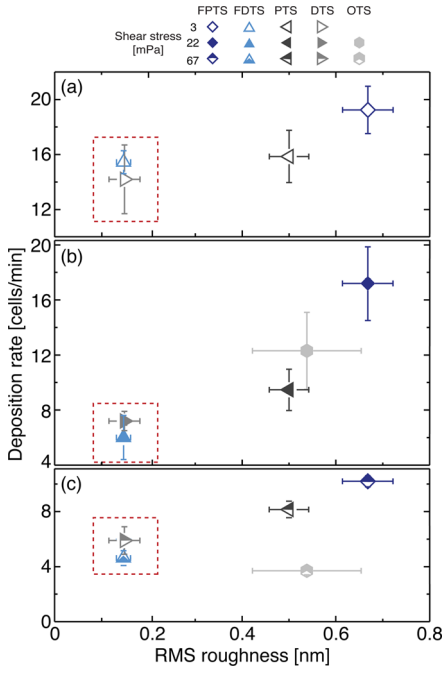

Figure 5. Deposition rate as a function of the rms surface roughness at shear stresses of (a) 3, (b) 22, and (c) 67 mPa. Error bars indicate standard deviation over at least three replicate measurements. The red boxes indicate the surfaces with roughness of less than 0.2 nm, on which cells exhibit mobile adhesion at all shear stresses investigated. The vertical scale is the same for each panel; the different shear stresses are separated for clarity. Strain: MC1061.

It is well known that increasing the surface roughness affects bacterial adhesion. Earlier studies of *E. coli* attachment in static cultures reported decreasing adhesion with increasing sub-nanometer-scale roughness[38] but increasing adhesion with increasing nanoscale roughness.[56,57] Smooth polymer (Vivathane) surfaces reduced the attachment of *E. coli* compared to that of other rougher biopolymer surfaces.[58] The increase in rms roughness observed on our silanized glass surfaces is comparable to that reported to reduce the adhesion of *E. coli* to nanostructured polyurethane surfaces under static conditions.[38] By contrast, we observe increasing bacterial adhesion with surface roughness on the subnanometer scale.

Near-Surface Motility. Next, we characterize the amount of motion exhibited by bacteria that closely associate with the substrate. In the microscopy movies, surface-associated bacteria exhibit motion in the form of small displacements of the centroid about a point of tether or site of attachment. In an earlier study, we showed that the rate at which bacteria attach to silane-functionalized surfaces varied inversely with the extent of this surface-associated motion.[19] To quantify the extent of surface-associated motion on the five test substrates, we define a metric based on the percentage of cells that undergo small displacements.[19] Briefly, we calculate the displacement of the centroid of each bacterium over each time step (Δt = 3 s) and calculate, as one metric of the extent of motility, the percentage of individual cell displacements that are larger than 0.12 μm (one pixel). The extent of motility, so defined, generally decreases for each surface with increasing shear stress (Figure 6a). Differences between motility on different silanes are most

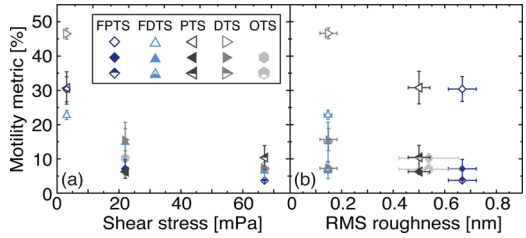

Figure 6. Extent of motility metric (percentage of individual cell displacements that are greater than 0.12 μm) as a function of (a) shear stress and (b) rms surface roughness. Symbol weights indicate the shear stress: open symbols, 3 mPa; closed symbols, 22 mPa; and half-open symbols, 67 mPa. Errors bars indicate the standard deviation over at least three replicate measurements. Strain: MC1061.

pronounced at the lowest shear stress studied (3 mPa) but become insignificant at the highest shear stress (67 mPa). These results suggest that, over the range of shear stresses studied, the surface-associated motion is affected more by shear stress than by surface chemistry. We next examine the dependence of the motility metric on the surface roughness. For a fixed shear stress, the extent of motility decreases slightly with increasing rms roughness (Figure 6b), opposing the trend seen for the deposition rate (Figure 5); this result is consistent with our earlier study[19] in which this motility metric was inversely correlated with the deposition rate.

In addition, we observe a second type of near-surface motion not seen in our earlier study. On DTS and FDTS surfaces, some bacteria very near the surface translate linearly along the direction of flow (Figure 7a and Movies S1, S3, and S4 in the Supporting Information). The maximum end-to-end linear displacements of these translating cells, 17 μm on FDTS surfaces and 47 μm on DTS surfaces, are much larger than the cell body dimensions. This long linear translation is qualitatively different from the surface-associated motion about a tethering point also seen on other surfaces of similar terminal chemistry (e.g., PTS, Figure 7b).

In an earlier study on *S. epidermidis*, the mobility associated with long linear displacements was termed slipping or mobile

DOI: 10.1021/acs.langmuir.6b00883
Langmuir 2016, 32, 5422−5433

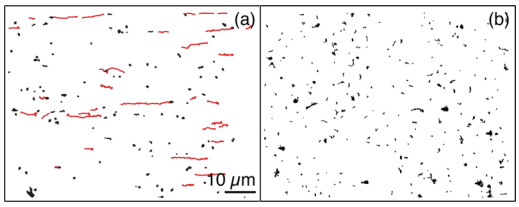

Figure 7. Representative trajectories of *E. coli* MC1061 bacteria on (a) a DTS-modified glass substrate (shear stress 22 mPa) and (b) a PTS-modified glass substrate (shear stress 3 mPa). Flow is from left to right. Trajectories in red correspond to bacteria exhibiting mobile adhesion, defined as a net linear displacement greater than 2.9 μm; all other trajectories are shown in black. Bacteria exhibit mobile adhesion on DTS but not on PTS surfaces. Scale bar = 10 μm.

adhesion.[29] Here, we identify a near-surface cell as exhibiting mobile adhesion if its net linear displacement in the direction of flow is greater than 2.9 μm. This displacement is greater than twice the maximum displacement observed for bacteria exhibiting surface-associated motion in our earlier study[19] and is approximately 1.5 times the length of an average *E. coli* bacterium obtained from our image-processing algorithms[53] (which slightly underestimate the cell length). Changing the cutoff by twice the resolution of the tracking algorithm does not change the identification of trajectories exhibiting mobile adhesion (Figure S6). We subsequently calculate the fraction of attached cells using mobile adhesion for each surface and for all flow rates. Between 2 and 15% of cells exhibit mobile adhesion on the DTS and FDTS surfaces, depending on the shear rate (Figure 8); by contrast, almost no cells on the other

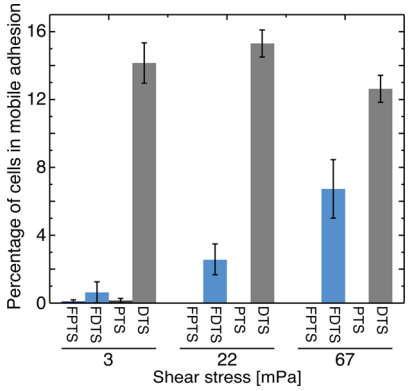

Figure 8. Percentage of attaching cells that exhibit mobile adhesion as a function of shear stress. Error bars indicate the standard deviation over three replicates. Strain: MC1061.

three surfaces (FPTS, PTS, and OTS) exhibit mobile adhesion. This finding suggests that mobile adhesion does not occur in response to a particular surface functional (chemical) group: it is observed on alkyl DTS but not on alkyl PTS or OTS. Similarly, it is observed on fluoroalkyl FDTS but not on fluoroalkyl FPTS.

To understand the factors that give rise to this near-surface mobility, we consider explanations proposed for transient or mobile adhesion in earlier studies. First, XPS analysis reveals no surface contaminants, indicating that chemical contamination does not give rise to mobile adhesion. Next, we consider explanations related to the wettability of the substrates. Earlier experiments on *S. epidermidis* reported that mobile adhesion was favored on hydrophilic substrates.[29] In that study, differences in the likelihood of mobile adhesion on hydrophobic and hydrophilic substrates were attributed to differences in the interaction of water with the surfaces. Bacteria exhibit attractive acid−base interactions with hydrophobic surfaces; as a result, water was readily displaced from the surface to allow bacteria to more closely approach it and establish immobile adhesion. By contrast, on hydrophilic surfaces there is a significant energy penalty to displace interfacial water, which inhibited the close approach of bacteria to these surfaces; cells that could not closely approach the surface were suggested to be more likely to exhibit mobile adhesion.[29] In our experiments, however, all surfaces are neutrally wetting or hydrophobic (Table 3). Nonetheless, we observe the mobile adhesion of *E. coli* on two of the four hydrophobic substrates, suggesting that hydrophilicity alone is not a sufficient condition for *E. coli* to exhibit mobile adhesion.

Third, we consider explanations related to specific cell−substrate interactions. Earlier reports of mobile or transient adhesion for *E. coli* attributed that mobility to specific chemical interactions between cell surface adhesins and functional groups on the substrate. For example, stick-and-roll adhesion of *E. coli* is mediated by force-dependent catch bonds between adhesins on the fimbriae and mannose or oligomannose groups on the surface.[40,41] Stick-and-roll adhesion was observed when fimbrial tip protein FimH specifically interacted with mannosylated bovine serum albumin on the surface. When the fluid shear stress was low (0.1−1 Pa), cells rolled at speeds of ∼30 μm/s across surfaces; at intermediate shear stresses (2−10 Pa), cells attached in the stationary state but resumed slow rolling at higher stresses (10 Pa).[15] In another set of experiments, 30−50% of bacteria exhibited rolling adhesion on 3-mannose-functionalized surfaces at shear stresses of 0.01−0.1 Pa; cells converted to stationary adhesion above 2 Pa.[59] In our experiments, however, mobile adhesion does not appear to require specific interactions between the cells and the surfaces. The DTS- and FDTS-modified glass surfaces used in our experiments present no known specific receptors for binding *E. coli* surface adhesins. Moreover, both the fraction of cells exhibiting mobile adhesion in our experiments (2−15%) and the speed at which they linearly translate (∼0.4 μm/s for shear stresses of 3−67 mPa) are smaller than those reported for interaction-mediated mobile (stick-and-roll) adhesion. These comparisons suggest that specific interactions are unlikely to give rise to the mobile adhesion observed here.

Instead, we note that one difference between the DTS and FDTS surfaces (on which we observe mobile adhesion) and FPTS, PTS, and OTS (on which we do not) is the rms roughness (Table 3). DTS and FDTS surfaces are very smooth, with rms roughnesses of less than 0.2 nm. By contrast, the other surfaces exhibit rms roughnesses of 0.5−0.7 nm, more than a factor of 2 greater. No other surface property neatly separates these two groups. Hence, we suggest that, because the mobile adhesion observed here occurs only on very smooth surfaces, it is a physicochemical rather than purely chemical response.

Although cells on both FDTS and DTS surfaces exhibit mobile adhesion, the two surfaces show somewhat different trends as the shear stress is increased. On FDTS surfaces, cells are more likely to use mobile adhesion as the shear stress is increased; by contrast, on DTS surfaces, the percentage of cells using this mode does not vary with shear stress (Figure 8). Given that the FDTS and DTS surfaces exhibit very similar water contact angles, zeta potentials, thicknesses, and roughness (but somewhat different surface energies), the origin of the

DOI: 10.1021/acs.langmuir.6b00883
Langmuir 2016, 32, 5422−5433

different trends is not clear; although the functional groups do not dictate whether mobile adhesion appears, interactions with specific functional groups may still affect the likelihood that cells use mobile adhesion in response to varying shear stress.

Characteristics of Mobile Adhesion. We first quantify the surface speed of mobile adhering cells from the centroid displacement of each bacterium over each time step (Δt = 3 s). On both FDTS and DTS surfaces, mobile adhesion is slow: the speed of cells (<0.4 μm/s) is significantly slower than both the average velocity of the applied flow (0.05−1.25 cm/s) and the typical near-surface swimming speed of *E. coli* (20−30 μm/s).[60] On both surfaces, the speed decreases as a function of applied shear stress (Figure 9; an explanation of the notched box plot is

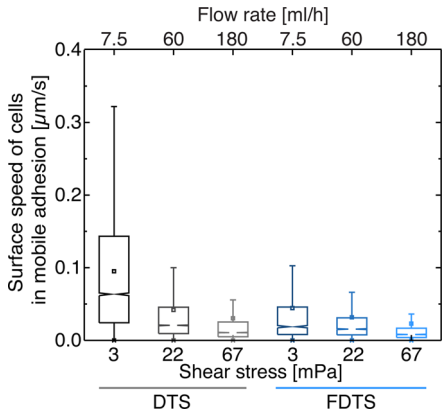

Figure 9. Distribution of the surface speed (calculated over a single time step of Δt = 3 s) of cells in mobile adhesion as a function of volumetric flow rate and shear stress. Number of data points in each speed distribution at volumetric flow rates of 7.5, 60, and 180 mL/h, respectively: DTS (N = 9538, 14 381, 7223) and FDTS (N = 1340, 3447, 5110). Notches on the box indicate the 95% confidence interval about the median value. The notches on the box plots above do not overlap for a given surface, indicating that the median values of the speed differ at the 95% confidence level. Strain: MC1061.

included as Figure S7 in the SI). This result runs counter to expectations from hydrodynamics; because shear stress increases the hydrodynamic force experienced by a surface-associated bacterium,[61] motions driven solely by hydrodynamic forces would be expected to increase with shear stress. Indeed, earlier studies of colloidal particles rolling on a surface found that their velocity increased from 4 to 14 μm/s and the distance rolled increased from <1.5 to >5 μm as the shear rate was increased from 20 to 50 s^{-1}.[62] Similarly, silica particles on electrostatically heterogeneous surfaces were more likely to persistently roll than to irreversibly arrest as the shear stress was increased.[63] Moreover, hydrodynamic colloidal models that predict the shear stresses required for particle detachment through sliding, rolling, or lifting mechanisms[64] or that relate particle detachment to surface and particle roughness[65,66] do not correlate to the experimentally observed mobile adhesion. These comparisons indicate that it is unlikely that mobile adhesion is purely hydrodynamic in origin; instead, we suggest that the slowing of mobile adherent cells in response to increasing shear stress reflects a combination of physicochemical and hydrodynamic interactions to resist detachment as the shear force is increased.

We next consider whether mobile adhesion helps cells to remain near the surface for long times; increased surface residence times could aid cells attempting to colonize environments featuring high shear stresses, with one example being the colonization of the urinary tract or of catheters embedded therein.[67,68] To test whether mobile adhesion allows cells to increase their surface dwell time, we calculated the residence times of each cell interacting with a DTS-functionalized surface, which exhibited the highest frequency of mobile adhesion and the largest cell displacements among all surfaces examined. The residence time of mobile adhering cells on DTS increases with shear stress, as shown in Figure 10, and the

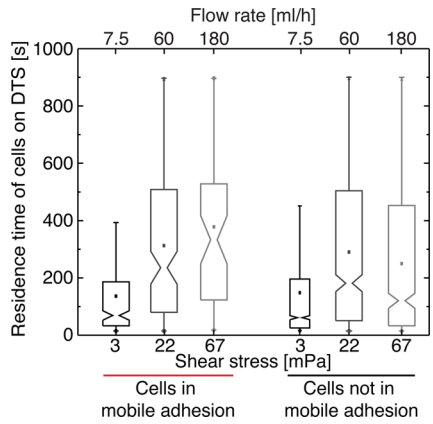

Figure 10. Residence time distribution of cells in mobile adhesion (left) and those not in mobile adhesion (right) on DTS. Notches represent the 95% confidence intervals. The (median) residence time of mobile adhering cells increases with shear stress, whereas that for cells not in mobile adhesion does not. Strain: MC1061.

increase in residence time between 3 and 22 mPa (but not between 22 and 67 mPa) is significant at the 95% confidence level. By contrast, the residence times for cells not in mobile adhesion are uncorrelated with the shear stress. This result suggests that mobile adhesion may enable cells to increase their residence time on the surface, which in turn could promote subsequent irreversible attachment.

Dependence of Mobile Adhesion on Flagella and Fimbriae. Mobile adhesion is observed only on very smooth surfaces. The dependence of mobile adhesion on the subnanoscale surface topography is somewhat surprising, as *E. coli* cells have a typical body length and diameter of ∼2 μm and ∼1 μm, respectively, which are both significantly larger than the measured nanoscale roughness of the silane surfaces. *E. coli* also possesses surface appendages and extracellular structures, of which two are widely studied and known to mediate attachment on biotic and abiotic surfaces:[17,30,69,70] fimbriae (5−7 nm wide and ∼1 μm long)[70] and flagella (∼20 nm wide and 5−10 μm long).[70] In addition, fimbriae mediate another kind of (faster) transient adhesion observed in *E. coli*, stick and roll, through specific interaction of the FimH adhesin with mannosylated surfaces.[17] We therefore hypothesize that these surface structures may affect whether *E. coli* cells exhibit mobile adhesion. To test this idea, we also perform deposition experiments using different derivatives of *E. coli* K-12: strain BW25113 and two isogenic mutants JW4277 (Δ*fimA*) and JW1908 (Δ*fliC*) that lack the ability to produce fimbriae and flagella, respectively; strain MG1655(Δ*fimA*), which lacks the ability to produce fimbriae (also of K-12 origin); and MG1655-pPCC1401, an engineered strain that overexpresses fimbriae upon induction with IPTG. The expression of flagella in the wild-type strains, in MG1655(Δ*fimA*) and in MG1655-

DOI: 10.1021/acs.langmuir.6b00883
Langmuir 2016, 32, 5422−5433

pPCC1401, and the lack of expression of flagella in the JW1908 strain, respectively, are confirmed through a motility assay and through transmission electron microscopy (TEM). TEM imaging of MC1061, BW25113, and its two mutants reveals that none of these strains express fimbriae and confirms that MG1655-pPCC1401 expresses fimbriae (Figure S3 in the Supporting Information) under the culture conditions used for deposition experiments.

To test the effects of these surface structures on mobile adhesion, we use DTS-coated surfaces and a single flow rate of 60 mL/h (corresponding to a shear stress of 22 mPa); these conditions produce the greatest number of mobile adherent cells in the first set of experiments with *E. coli* MC1061 (Figure 8). We observe mobile adhesion for BW25113 and its mutants (Figure 11) and also for MG1655Δ*fimA*, none of which express

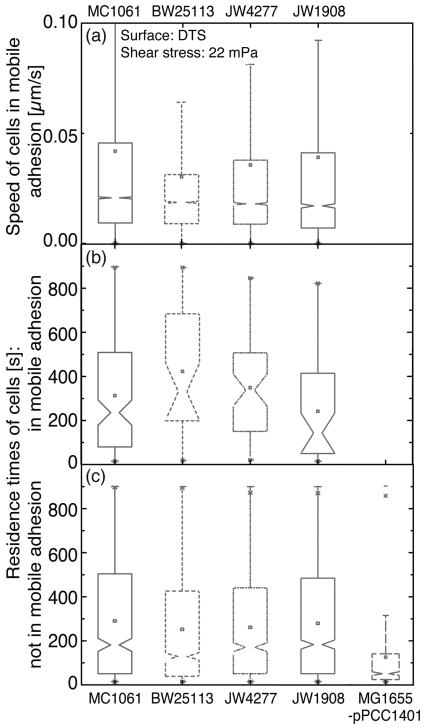

Figure 11. Effects of surface adhesins on the mobile adhesion of *E. coli* cells flowing at 60 mL/h (shear stress: 22 mPa) on DTS-functionalized surfaces. (a) Distribution of the instantaneous speed of bacteria in mobile adhesion on DTS at 22 mPa for *E. coli* K-12 strains MC1061 (wild type) and BW25113 (wild type) and isogenic mutants JW4277 and JW1908. (b) Distributions of residence times of bacteria in mobile adhesion. Notches on the box plot represent a 95% confidence interval about the mean. The 95% confidence intervals for *E. coli* strain BW25113 and its isogenic mutants JW4277 and JW1908 overlap, indicating that the instantaneous speeds and residence times for these cells do not differ at this confidence level. (c) Distribution of residence times for cells not exhibiting mobile adhesion (for five bacterial strains) on DTS at 22 mPa.

fimbriae (Figure S3 in the Supporting Information), but we do not observe mobile adhesion on DTS surfaces for fimbriated strain MG1655-pPCC1401. This result suggests that lack of fimbriae is a necessary condition for mobile adhesion. The frequency of mobile adhesion observed in BW25113 and its mutants is comparable but is approximately half that observed for MC1061 on DTS at 22 mPa shear stress. MC1061 and BW25113, however, are two different derivatives of *E. coli* K-12 and bear distinct genetic mutations that may contribute to differences in cell−surface interactions.

Our results suggest that nanoscale surface roughness plays a critical role in the attachment of bacteria on surfaces that do not present specific interaction sites for adhesion. On very smooth surfaces (of roughness below 0.2 nm) and in the absence of fimbriae expression, bacteria in our experiments exhibit mobile adhesion until they either become irreversibly adhered or detach from the surface. Although the differences in roughness are significantly smaller than the dimensions of the cell body, the maximum peak-to-valley height on the silane surfaces (1.4 to 5.6 nm) is comparable to the width of fimbriae and other shorter cell surface adhesins. Therefore, we suggest that changes in bacterial adhesion on surfaces with sub-nanometer-scale roughness arise from interactions of bacterial surface adhesins with the roughness. Hence mobile adhesion occurs for smooth (fimbriae-deficient) bacteria on smooth (minimally rough) surfaces, suggesting that reduced frictional interactions give rise to this motility behavior. Although reports of nonspecific and non-appendage-driven bacterial transient motility are rare, two earlier studies relate transient bacterial motility to frictional interactions. First, frictional forces acting laterally along the substratum were suggested to induce a transition from mobile to immobile adhesion of *S. epidermidis* on soft and rigid polymer brushes.[43] Second, a theoretical study on the deposition of *Streptococcus oralis* on an ideally smooth surface predicted mobile adhesion arising from the absence of lateral interactions that cause immobilization.[44]

Although the metaphor of friction unifies the two requirements for mobile adhesion (smooth surfaces and a lack of fimbriae), one result cannot be explained by such a simple picture: over the limited range of stress probed, increasing shear stress increases the residence time of cells in mobile adhesion. This enhancement is greater than that observed for cells not in mobile adhesion (Figure 10). Specific (fimH-mediated) interactions between cells and substrates weaken over this range of shear stresses and cannot explain this enhancement.[41] Instead, our results appear to be consistent with an earlier report of (apparently) nonspecific shear-enhanced adhesion in *Pseudomonas aeruginosa*.[42] In that study, the shear-enhanced increase in residence time could not be linked to a specific interaction; it was independent of the substrate and not mediated by type I pili, type IV pili, flagella, or the extracellular matrix. Hence we suggest that the slight increase in residence time for our cells also originates from an as-yet unidentified stress-sensitive mechanism.

CONCLUSIONS

We characterized near-surface motility associated with adhesion in *E. coli* bacteria deposited from flow on glass substrates bearing self-assembled alkylsilane and fluoroalkylsilane films. By analyzing the trajectories of hundreds of bacteria deposited on these surfaces, we found that the deposition rate for all surfaces generally decreased with increasing shear stress. The discrepancy between the predicted xDLVO interaction potentials and the observed relative deposition rates suggested that other interactions influenced deposition. We found that the deposition rate increased approximately linearly with the rms surface roughness. Similarly, the extent of surface-associated motion decreased with rms roughness, consistent with greater cell adhesion to the rougher surfaces. Cells exhibited mobile adhesion on very smooth surfaces undergoing large linear displacements. As the shear stress was increased, the speed of

DOI: 10.1021/acs.langmuir.6b00883
Langmuir 2016, 32, 5422−5433

mobile adhesion decreased and the residence time of cells increased. In contrast to earlier reports of near-surface transient adhesion in *E. coli*,[15,71,72] mobile adhesion did not involve specific interactions between bacterial adhesins and the surface. Instead, only cells that did not express fimbriae exhibited mobile adhesion. Because mobile adhesion required very smooth surfaces as well as the absence of the adhesive fimbriae, we suggest that this mode reflects reduced friction between cells and surfaces and hence arises from a physical origin. This is in contrast to most known modes of near-surface motility, which are driven directly by appendages[60,73] or indirectly by specific interactions.[15,74]

The effects reported here do not apparently depend on active processes of the bacteria but only on roughness, which is known to influence the deposition and transient adhesion of abiotic microscale particles. For example, both theoretical and experimental studies of colloidal deposition on surfaces of varying roughness indicate that rough surfaces are more favorable for particle deposition.[75−77] These studies proposed that the increase in deposition arose from a reduction in the repulsive energy barrier with increased roughness and/or attractive colloidal and steric interactions that are absent for smooth surfaces.[76,77] Similarly, the rolling adhesion of colloidal particles depends on nanometer-scale surface chemical/charge heterogeneities.[63,78] With an increasing density of surface heterogeneity (charge), the particle motion switched from dynamic rolling to sudden arrest without particle deceleration.[63] This observation is similar to our finding that surface roughness (i.e., heterogeneity in surface topography) determines the transition from mobile to immobile adhesion for bacteria.

Initial cell−surface interactions are thought to affect the growth and composition of biofilms.[79] Reducing frictional interactions between cells and surfaces, either by engineering nanoscale-smooth surfaces or by suppressing the expression of cell−surface adhesins, may help to reduce fouling during initial deposition. After the initial surface interaction, however, mobile adhesion increases the residence time of cells near surfaces; this behavior may help cells to resist detachment and hence promote *E. coli* biofilm formation in settings in which cells are exposed to varying and/or high shear stresses, such as in bioreactors[80] or on medical implants.[34] In the later stages of biofilm formation, however, cells excrete extracellular polymeric substances that condition the surface and promote surface attachment. Hence we expect that strategies to reduce frictional interactions will be most effective in the very earliest stages at which cells initially encounter surfaces.

■ ASSOCIATED CONTENT

Supporting Information

The Supporting Information is available free of charge on the ACS Publications website at DOI: 10.1021/acs.langmuir.6b00883.

Descriptions of movies of bacterial deposition and supporting results on bacterial growth curves, flagella and fimbriae expression assays, TEM images, XPS results and analysis, extended DLVO calculations, atomic force microscopy results and discussion, and the O'Neill shear force acting on attached bacteria (PDF)

Deposition of *E. coli* MC1061 on DTS-modified glass showing the mobile adhesion of cells on the surface and immobile surface association (AVI)

Deposition of *E. coli* MC1061 on PTS-modified glass showing the absence of mobile adhesion (AVI)

Deposition of *E. coli* MC1061 on FDTS-modified glass showing the mobile adhesion of cells on the surface and immobile surface association (AVI)

Deposition of *E. coli* MG1655Δ*fimA* on DTS-modified glass showing the mobile adhesion of cells on the surface and immobile surface association (AVI)

■ AUTHOR INFORMATION

Corresponding Author

*E-mail: jcconrad@uh.edu.

Author Contributions

S.S. and Y.A.J.-L. contributed equally.

Notes

The authors declare no competing financial interest.

■ ACKNOWLEDGMENTS

We acknowledge support from the National Science Foundation (DMR-1151133) and the Welch Foundation (E-1869). We thank Dr. Evgeni Sokurenko and Dr. Wendy Thomas (University of Washington) for the PAb49 antibody; Dr. Richard Willson (UH) for access to bacteria culture equipment; Dr. Gila Stein (UH) for access to ellipsometry and goniometry instruments; Dr. Peter Vekilov (UH) for access to the AFM instrument; Dr. Boris Makarenko (UH) for XPS measurements; and Dr. Michael Wong (Rice University) for the use of his zeta potential instrument.

■ REFERENCES

(1) Neria-González, I.; Wang, E. T.; Ramírez, F.; Romero, J. M.; Hernández-Rodríguez, C. Characterization of bacterial community associated to biofilms of corroded oil pipelines from the southeast of Mexico. *Anaerobe* **2006**, *12*, 122−133.

(2) Tribou, M.; Swain, G. The use of proactive in-water grooming to improve the performance of ship hull antifouling coatings. *Biofouling* **2010**, *26*, 47−56.

(3) Chmielewski, R. A. N.; Frank, J. F. Biofilm formation and control in food processing facilities. *Compr. Rev. Food Sci. Food Saf.* **2003**, *2*, 22−32.

(4) Donlan, R. M. Biofilm formation: a clinically relevant microbiological process. *Clin. Infect. Dis.* **2001**, *33*, 1387−1392.

(5) Costerton, J. W. Cystic fibrosis pathogenesis and the role of biofilms in persistent infection. *Trends Microbiol.* **2001**, *9*, 50−52.

(6) Bosio, S.; Leekha, S.; Gamb, S. I.; Wright, A. J.; Terrell, C. L.; Miller, D. V. *Mycobacterium fortuitum* prosthetic valve endocarditis: a case for the pathogenetic role of biofilms. *Cardiovasc. Pathol.* **2012**, *21*, 361−364.

(7) Von Rosenvinge, E. C.; O'May, G. A.; Macfarlane, S.; Macfarlane, G. T.; Shirtliff, M. E. Microbial biofilms and gastrointestinal diseases. *Pathog. Dis.* **2013**, *67*, 25−38.

(8) García, C.; Moreno, D. A.; Ballester, A.; Blázquez, M. L.; González, F. Bioremediation of an industrial acid mine water by metal-tolerant sulphate-reducing bacteria. *Miner. Eng.* **2001**, *14*, 997−1008.

(9) Pearce, C. I.; Lloyd, J. R.; Guthrie, J. T. The removal of colour from textile wastewater using whole bacterial cells: a review. *Dyes Pigm.* **2003**, *58*, 179−196.

(10) Bouwer, E. J.; Zehnder, A. J. B. Bioremediation of organic compounds - putting microbial metabolism to work. *Trends Biotechnol.* **1993**, *11*, 360−367.

(11) Singh, R.; Paul, D.; Jain, R. K. Biofilms: implications in bioremediation. *Trends Microbiol.* **2006**, *14*, 389−397.

(12) van Oss, C. J. The forces involved in bioadhesion to flat surfaces and particles — Their determination and relative roles. *Biofouling* **1991**, *4*, 25−35.

DOI: 10.1021/acs.langmuir.6b00883
Langmuir 2016, 32, 5422−5433

(13) Hermansson, M. The DLVO theory in microbial adhesion. *Colloids Surf., B* **1999**, *14*, 105−119.
(14) Lund, B.; Lindberg, F.; Marklund, B. I.; Normark, S. The PapG protein is the alpha-D-galactopyranosyl-(1—4)-beta-D-galactopyranose-binding adhesin of uropathogenic *Escherichia coli*. *Proc. Natl. Acad. Sci. U. S. A.* **1987**, *84*, 5898−5902.
(15) Thomas, W. E.; Nilsson, L. M.; Forero, M.; Sokurenko, E. V.; Vogel, V. Shear-dependent 'stick-and-roll' adhesion of type 1 fimbriated *Escherichia coli*. *Mol. Microbiol.* **2004**, *53*, 1545−1557.
(16) Pratt, L. A.; Kolter, R. Genetic analyses of bacterial biofilm formation. *Curr. Opin. Microbiol.* **1999**, *2*, 598−603.
(17) Van Houdt, R.; Michiels, C. W. Role of bacterial cell surface structures in *Escherichia coli* biofilm formation. *Res. Microbiol.* **2005**, *156*, 626−633.
(18) Cunliffe, D.; Smart, C. A.; Alexander, C.; Vulfson, E. N. Bacterial adhesion at synthetic surfaces. *Appl. Environ. Microbiol.* **1999**, *65*, 4995−5002.
(19) Sharma, S.; Conrad, J. C. Attachment from flow of *Escherichia coli* bacteria onto silanized glass substrates. *Langmuir* **2014**, *30*, 11147−11155.
(20) Harden, V. P.; Harris, J. O. The isoelectric point of bacterial cells. *J. Bacteriol.* **1953**, *65*, 198−202.
(21) Van Loosdrecht, M. C.; Lyklema, J.; Norde, W.; Schraa, G.; Zehnder, A. J. Electrophoretic mobility and hydrophobicity as a measured to predict the initial steps of bacterial adhesion. *Appl. Environ. Microbiol.* **1987**, *53*, 1898−1901.
(22) Rose, S. F.; Okere, S.; Hanlon, G. W.; Lloyd, A. W.; Lewis, A. L. Bacterial adhesion to phosphorylcholine-based polymers with varying cationic charge and the effect of heparin pre-adsorption. *J. Mater. Sci.: Mater. Med.* **2005**, *16*, 1003−1015.
(23) Ong, Y.-L.; Razatos, A.; Georgiou, G.; Sharma, M. M. Adhesion forces between *E. coli* bacteria and biomaterial surfaces. *Langmuir* **1999**, *15*, 2719−2725.
(24) Absolom, D. R.; Lamberti, F. V.; Policova, Z.; Zingg, W.; van Oss, C. J.; Neumann, A. W. Surface thermodynamics of bacterial adhesion. *Appl. Environ. Microbiol.* **1983**, *46*, 90−97.
(25) Tuson, H. H.; Weibel, D. B. Bacteria-surface interactions. *Soft Matter* **2013**, *9*, 4368−4380.
(26) Park, K. D.; Kim, Y. S.; Han, D. K.; Kim, Y. H.; Lee, E. H. B.; Suh, H.; Choi, K. S. Bacterial adhesion on PEG modified polyurethane surfaces. *Biomaterials* **1998**, *19*, 851−859.
(27) Cerca, N.; Pier, G. B.; Vilanova, M.; Oliveira, R.; Azeredo, J. Quantitative analysis of adhesion and biofilm formation on hydrophilic and hydrophobic surfaces of clinical isolates of Staphylococcus epidermidis. *Res. Microbiol.* **2005**, *156*, 506−514.
(28) Roosjen, A.; de Vries, J.; van der Mei, H. C.; Norde, W.; Busscher, H. J. Stability and effectiveness against bacterial adhesion of poly(ethylene oxide) coatings in biological fluids. *J. Biomed. Mater. Res., Part B* **2005**, *73B*, 347−354.
(29) Boks, N. P.; Kaper, H. J.; Norde, W.; van der Mei, H. C.; Busscher, H. J. Mobile and immobile adhesion of staphylococcal strains to hydrophilic and hydrophobic surfaces. *J. Colloid Interface Sci.* **2009**, *331*, 60−64.
(30) Friedlander, R. S.; Vlamakis, H.; Kim, P.; Khan, M.; Kolter, R.; Aizenberg, J. Bacterial flagella explore microscale hummocks and hollows to increase adhesion. *Proc. Natl. Acad. Sci. U. S. A.* **2013**, *110*, 5624−5629.
(31) Poncin-Epaillard, F.; Herry, J. M.; Marmey, P.; Legeay, G.; Debarnot, D.; Bellon-Fontaine, M. N. Elaboration of highly hydrophobic polymeric surface — a potential strategy to reduce the adhesion of pathogenic bacteria? *Mater. Sci. Eng., C* **2013**, *33*, 1152−1161.
(32) Taylor, R. L.; Verran, J.; Lees, G. C.; Ward, A. J. P. The influence of substratum topography on bacterial adhesion to polymethyl methacrylate. *J. Mater. Sci.: Mater. Med.* **1998**, *9*, 17−22.
(33) Sousa, C.; Rodrigues, D.; Oliveira, R.; Song, W.; Mano, J. F.; Azeredo, J. Superhydrophobic poly(L-lactic acid) surface as potential bacterial colonization substrate. *AMB Express* **2011**, *1*, 34.
(34) Truong, V. K.; Lapovok, R.; Estrin, Y. S.; Rundell, S.; Wang, J. Y.; Fluke, C. J.; Crawford, R. J.; Ivanova, E. P. The influence of nano-scale surface roughness on bacterial adhesion to ultrafine-grained titanium. *Biomaterials* **2010**, *31*, 3674−3683.
(35) Etxeberria, M.; López-Jiménez, L.; Merlos, A.; Escuín, T.; Viñas, M. Bacterial adhesion efficiency on implant abutments: A comparative study. *Int. Microbiol.* **2013**, *16*, 235−242.
(36) Bruinsma, G. M.; Rustema-Abbing, M.; de Vries, J.; Busscher, H. J.; van der Linden, M. L.; Hooymans, J. M. M.; van der Mei, H. C. Multiple surface properties of worn RGP lenses and adhesion of *Pseudomonas aeruginosa*. *Biomaterials* **2003**, *24*, 1663−1670.
(37) Mitik-Dineva, N.; Wang, J.; Mocanasu, R. C.; Stoddart, P. R.; Crawford, R. J.; Ivanova, E. P. Impact of nano-topography on bacterial attachment. *Biotechnol. J.* **2008**, *3*, 536−544.
(38) Yao, C.; Webster, T. J.; Hedrick, M. Decreased bacteria density on nanostructured polyurethane. *J. Biomed. Mater. Res., Part A* **2014**, *102*, 1823−1828.
(39) Ivanova, E. P.; Truong, V. K.; Webb, H. K.; Baulin, V. A.; Wang, J. Y.; Mohammodi, N.; Wang, F.; Fluke, C.; Crawford, R. J. Differential attraction and repulsion of *Staphylococcus aureus* and *Pseudomonas aeruginosa* on molecularly smooth titanium films. *Sci. Rep.* **2011**, *1*, 165.
(40) Thomas, W.; Trintchina, E.; Forero, M.; Vogel, V.; Sokurenko, E. V. Bacterial adhesion to target cells enhanced by shear force. *Cell* **2002**, *109*, 913−923.
(41) Nilsson, L.; Thomas, W.; Trintchina, E.; Vogel, V.; Sokurenko, E. Catch bond-mediated adhesion without a shear threshold: trimannose versus monomannose interactions with the FimH adhesin of *Escherichia coli*. *J. Biol. Chem.* **2006**, *281*, 16656−16663.
(42) Lecuyer, S.; Rusconi, R.; Shen, Y.; Forsyth, A.; Vlamakis, H.; Kolter, R.; Stone, H. A. Shear stress increases the residence time of adhesion of *Pseudomonas aeruginosa*. *Biophys. J.* **2011**, *100*, 341−350.
(43) Swartjes, J. J. T. M.; Veeregowda, D. H.; van der Mei, H. C.; Busscher, H. J.; Sharma, P. K. Normally oriented adhesion versus friction forces in bacterial adhesion to polymer-brush functionalized surfaces under fluid flow. *Adv. Funct. Mater.* **2014**, *24*, 4435−4441.
(44) Busscher, H. J.; Poortinga, A. T.; Bos, R. Lateral and perpendicular interaction forces involved in mobile and immobile adhesion of microorganisms on model solid surfaces. *Curr. Microbiol.* **1998**, *37*, 319−323.
(45) Fadeeva, E.; Truong, V. K.; Stiesch, M.; Chichkov, B. N.; Crawford, R. J.; Wang, J.; Ivanova, E. P. Bacterial retention on superhydrophobic titanium surfaces fabricated by femtosecond laser ablation. *Langmuir* **2011**, *27*, 3012−3019.
(46) Xu, H.; Murdaugh, A. E.; Chen, W.; Aidala, K. E.; Ferguson, M. A.; Spain, E. M.; Núñez, M. E. Characterizing pilus-mediated adhesion of biofilm-forming *E. coli* to chemically diverse surfaces using atomic force microscopy. *Langmuir* **2013**, *29*, 3000−3011.
(47) Baba, T.; Ara, T.; Hasegawa, M.; Takai, Y.; Okumura, Y.; Baba, M.; Datsenko, K. A.; Tomita, M.; Wanner, B. L.; Mori, H. Construction of *Escherichia coli* K-12 in-frame, single-gene knockout mutants: the Keio collection. *Mol. Syst. Biol.* **2006**, *2*, 1−11.
(48) Tang, S. Y.; Qian, S.; Akinterinwa, O.; Frei, C. S.; Gredell, J. A.; Cirino, P. C. Screening for Enhanced Triacetic Acid Lactone Production by Recombinant *Escherichia coli* Expressing a Designed Triacetic Acid Lactone Reporter. *J. Am. Chem. Soc.* **2013**, *135*, 10099−10103.
(49) Walker, S. L.; Redman, J. A.; Elimelech, M. Influence of growth phase on bacterial deposition: interaction mechanisms in packed-bed column and radial stagnation point flow systems. *Environ. Sci. Technol.* **2005**, *39*, 6405−6411.
(50) Tittsler, R. P.; Sandholzer, L. A. The use of semi-solid agar for the detection of bacterial motility. *J. Bacteriol.* **1936**, *31*, 575−580.
(51) van Oss, C. J. Acid—base interfacial interactions in aqueous media. *Colloids Surf., A* **1993**, *78*, 1−49.
(52) Zhou, W.; Zhang, J.; Liu, Y.; Li, X.; Niu, X.; Song, Z.; Min, G.; Wan, Y.; Shi, L.; Feng, S. Characterization of anti-adhesive self-assembled monolayer for nanoimprint lithography. *Appl. Surf. Sci.* **2008**, *255*, 2885−2889.

DOI: 10.1021/acs.langmuir.6b00883
Langmuir 2016, 32, 5422−5433

(53) Gibiansky, M. L.; Conrad, J. C.; Jin, F.; Gordon, V. D.; Motto, D. A.; Mathewson, M. A.; Stopka, W. G.; Zelasko, D. C.; Shrout, J. D.; Wong, G. C. L. Bacteria use type IV pili to walk upright and detach from surfaces. *Science* **2010**, *330*, 197.
(54) Chen, J.-K.; Ko, F.-H.; Hsieh, K.-F.; Chou, C.-T.; Chang, F.-C. Effect of fluoroalkyl substituents on the reactions of alkylchlorosilanes with mold surfaces for nanoimprint lithography. *J. Vac. Sci. Technol., B: Microelectron. Process. Phenom.* **2004**, *22*, 3233−3241.
(55) Castillo, J. M.; Klos, M.; Jacobs, K.; Horsch, M.; Hasse, H. Characterization of alkylsilane self-assembled monolayers by molecular simulation. *Langmuir* **2015**, *31*, 2630−2638.
(56) Singh, A. V.; Vyas, V.; Patil, R.; Sharma, V.; Scopelliti, P. E.; Bongiorno, G.; Podestà, A.; Lenardi, C.; Gade, W. N.; Milani, P. Quantitative characterization of the influence of the nanoscale morphology of nanostructured surfaces on bacterial adhesion and biofilm formation. *PLoS One* **2011**, *6*, e25029.
(57) Hsu, L. C.; Fang, J.; Borca-Tasciuc, D. A.; Worobo, R. W.; Moraru, C. I. Effect of micro- and nanoscale topography on the adhesion of bacterial cells to solid surfaces. *Appl. Environ. Microbiol.* **2013**, *79*, 2703−2712.
(58) McAllister, E. W.; Carey, L. C.; Brady, P. G.; Heller, R.; Kovacs, S. G. The role of polymeric surface smoothness of biliary stents in bacterial adherence, biofilm deposition, and stent occlusion. *Gastrointest. Endosc.* **1993**, *39*, 422−425.
(59) Anderson, B. N.; Ding, A. M.; Nilsson, L. M.; Kusuma, K.; Tchesnokova, V.; Vogel, V.; Sokurenko, E. V.; Thomas, W. E. Weak rolling adhesion enhances bacterial surface colonization. *J. Bacteriol.* **2007**, *189*, 1794−1802.
(60) Lauga, E.; DiLuzio, W. R.; Whitesides, G. M.; Stone, H. A. Swimming in circles: motion of bacteria near solid boundaries. *Biophys. J.* **2006**, *90*, 400−412.
(61) Boks, N. P.; Norde, W.; van der Mei, H. C.; Busscher, H. J. Forces involved in bacterial adhesion to hydrophilic and hydrophobic surfaces. *Microbiology* **2008**, *154*, 3122−3133.
(62) Whitehead, K. A.; Rogers, D.; Colligon, J.; Wright, C.; Verran, J. Use of the atomic force microscope to determine the effect of substratum surface topography on the ease of bacterial removal. *Colloids Surf., B* **2006**, *51*, 44−53.
(63) Kalasin, S.; Santore, M. M. Engineering nanoscale surface features to sustain microparticle rolling in flow. *ACS Nano* **2015**, *9*, 4706−4716.
(64) Hubbe, M. A. Theory of detachment of colloidal particles from flat surfaces exposed to flow. *Colloids Surf.* **1984**, *12*, 151−178.
(65) Burdick, G. M.; Berman, N. S.; Beaudoin, S. P. Hydrodynamic particle removal from surfaces. *Thin Solid Films* **2005**, *488*, 116−123.
(66) Burdick, G. M.; Berman, N. S.; Beaudoin, S. P. Describing hydrodynamic particle removal from surfaces using the particle Reynolds number. *J. Nanopart. Res.* **2001**, *3*, 453−465.
(67) Kucheria, R.; Dasgupta, P.; Sacks, S. H.; Khan, M. S.; Sheerin, N. S. Urinary tract infections: new insights into a common problem. *Postgrad. Med. J.* **2005**, *81*, 83−86.
(68) Wiles, T. J.; Kulesus, R. R.; Mulvey, M. A. Origins and virulence mechanisms of uropathogenic *Escherichia coli*. *Exp. Mol. Pathol.* **2008**, *85*, 11−19.
(69) Díaz, C.; Schilardi, P. L.; dos Santos Claro, P. C.; Salvarezza, R. C.; Fernández Lorenzo de Mele, M. A. Submicron trenches reduce the *Pseudomonas fluorescens* colonization rate on solid surfaces. *ACS Appl. Mater. Interfaces* **2009**, *1*, 136−143.
(70) Feng, G.; Cheng, Y.; Wang, S.-Y.; Borca-Tasciuc, D. A.; Worobo, R. W.; Moraru, C. I. Bacterial attachment and biofilm formation on surfaces are reduced by small-diameter nanoscale pores: how small is small enough? *NPJ. Biofilms Microbiomes* **2015**, *1*, 15022.
(71) Thomas, W.; Forero, M.; Yakovenko, O.; Nilsson, L. M.; Vicini, P.; Sokurenko, E. V.; Vogel, V. Catch-bond model derived from allostery explains force-activated bacterial adhesion. *Biophys. J.* **2006**, *90*, 753−764.
(72) Sokurenko, E. V.; Vogel, V.; Thomas, W. E. Catch-bond mechanism of force-enhanced adhesion: counterintuitive, elusive, but··· widespread? *Cell Host Microbe* **2008**, *4*, 314−323.
(73) Berke, A. P.; Turner, L.; Berg, H. C.; Lauga, E. Hydrodynamic attraction of swimming microorganisms by surfaces. *Phys. Rev. Lett.* **2008**, *101*, 038102.
(74) Forero, M.; Thomas, W.; Bland, C.; Nilsson, L. M.; Sokurenko, E. V.; Vogel, V. A catch-bond based nanoadhesive sensitive to shear stress. *Nano Lett.* **2004**, *4*, 1593−1597.
(75) Kostoglou, M.; Karabelas, A. J. Effect of roughness on energy of repulsion between colloidal surfaces. *J. Colloid Interface Sci.* **1995**, *171*, 187−199.
(76) Suresh, L.; Walz, J. Y. Effect of surface roughness on the interaction energy between a colloidal sphere and a flat plate. *J. Colloid Interface Sci.* **1996**, *183*, 199−213.
(77) Hoek, E. M. V.; Bhattacharjee, S.; Elimelech, M. Effect of membrane surface roughness on colloid−membrane DLVO interactions. *Langmuir* **2003**, *19*, 4836−4847.
(78) Kalasin, S.; Santore, M. M. Hydrodynamic crossover in dynamic microparticle adhesion on surfaces of controlled nanoscale heterogeneity. *Langmuir* **2008**, *24*, 4435−4438.
(79) Busscher, H. J.; van der Mei, H. C. Physico-chemical interactions in initial microbial adhesion and relevance for biofilm formation. *Adv. Dent. Res.* **1997**, *11*, 24−32.
(80) Anselme, K.; Davidson, P.; Popa, A. M.; Giazzon, M.; Liley, M.; Ploux, L. The interaction of cells and bacteria with surfaces structured at the nanometre scale. *Acta Biomater.* **2010**, *6*, 3824−3846.

DOI: 10.1021/acs.langmuir.6b00883
Langmuir 2016, 32, 5422−5433